HHS Public Access

Author manuscript

*Cell Metab*. Author manuscript; available in PMC 2020 May 07.

Published in final edited form as:

*Cell Metab*. 2019 May 07; 29(5): 1206–1216.e4. doi:10.1016/j.cmet.2019.01.024.

# Differential metabolic reprogramming by Zika virus promotes cell death in human versus mosquito cells

**Shivani K. Thaker**[1,2], **Travis Chapa**[2], **Gustavo Garcia Jr.**[2], **Danyang Gong**[2], **Ernst W. Schmid**[1], **Vaithilingaraja Arumugaswami**[2,3,4], **Ren Sun**[2,5,6,*], **Heather R. Christofk**[1,2,3,5,7,*]

[1]Department of Biological Chemistry, David Geffen School of Medicine, University of California, Los Angeles, Los Angeles, CA 90095, USA

[2]Department of Molecular and Medical Pharmacology, David Geffen School of Medicine, University of California, Los Angeles, Los Angeles, CA 90095, USA

[3]Eli and Edythe Broad Center of Regenerative Medicine and Stem Cell Research, University of California, Los Angeles, Los Angeles, CA 90095, USA

[4]Department of Surgery, Cedars-Sinai Medical Center, Los Angeles, Los Angeles, CA 90098, USA

[5]UCLA Jonsson Comprehensive Cancer Center, David Geffen School of Medicine, University of California, Los Angeles, Los Angeles, CA 90095, USA

[6]Department of Bioengineering, Samueli School of Engineering, University of California, Los Angeles, Los Angeles, CA 90095, USA

[7]Lead Contact

## SUMMARY

Zika virus is a pathogen that poses serious consequences including congenital microcephaly. Although many viruses reprogram host cell metabolism, whether Zika virus alters cellular metabolism and the functional consequences of Zika-induced metabolic changes remain unknown. Here we show that Zika virus infection differentially reprograms glucose metabolism in human versus C6/36 mosquito cells by increasing glucose use in the tricarboxylic acid cycle in human cells, versus increasing glucose use in the pentose phosphate pathway in mosquito cells. Infection of human cells selectively depletes nucleotide triphosphate levels, leading to elevated AMP/ATP ratios, AMP-activated protein kinase (AMPK) phosphorylation, and caspase-mediated cell death. AMPK is also phosphorylated in Zika virus-infected mouse brain. Inhibiting AMPK in human cells decreases Zika virus-mediated cell death, whereas activating AMPK in mosquito cells promotes Zika virus-mediated cell death. These findings suggest the differential metabolic reprogramming during Zika virus infection of human versus mosquito cells determines whether cell death occurs.

*Correspondence: rsun@mednet.ucla.edu and hchristofk@mednet.ucla.edu.

AUTHOR CONTRIBUTIONS

S.K.T., T.C., R.S., and H.R.C. designed the study. S.K.T. and H.R.C. wrote the manuscript. S.K.T., T.C., G.G., D.G., and E.S. performed experiments. H.R.C., R.S., and V.A. supervised the project. All authors edited the manuscript.

DECLARATION OF INTERESTS

The authors declare no competing interests.

## INTRODUCTION

Zika virus (ZIKV), a member of the *Flaviviridae* family, is an emerging public health concern. Though the virus was first isolated in 1947, several outbreaks have occurred since that time, most notably in Brazil, the Americas, and parts of Asia and Africa beginning in 2015, leading the World Health Organization to declare ZIKV as a global public health emergency in 2016 (Baud, Gubler et al. 2017). While ZIKV infection typically leads to mild clinical symptoms, the virus can also cause a range of more severe symptoms including Guillain-Barré in adults and devastating outcomes including microcephaly and congenital brain defects in fetuses of infected mothers (de Oliveira, Carmo et al. 2017).

Studies over the past two years have begun to examine the mechanisms underlying ZIKV tropism and pathology. As an arthropod-borne virus, the urban transmission cycle of ZIKV involves replication in both mosquito vectors as well as humans (Petersen, Jamieson et al. 2016) (Saiz, Vazquez-Calvo et al. 2016). In humans, ZIKV shows broad tropism including neuronal cell types, placental cells, cells of the reproductive tract, endothelial cells, and ocular tissue (Miner and Diamond 2017). ZIKV infection of fetal neural stem cells and neuronal progenitor cells leads to caspase-mediated cell death and resulting neurodevelopmental deficits (Liang, Luo et al. 2016) (Tang, Hammack et al. 2016). Additionally, ZIKV has been shown to infect peripheral neurons and induce apoptotic cell death (Oh, Zhang et al. 2017). While ZIKV pathogenesis may be in part be due to death of infected cells, the mechanism by which apoptosis occurs during ZIKV infection is currently unknown. Unlike ZIKV-infected human cells, mosquito vectors infected with flaviviruses are viral reservoirs for their lifespans without experiencing any adverse health effects (Daep, Munoz-Jordan et al. 2014). The molecular mechanisms underlying the differential fate observed between ZIKV-infected host human cells and vector mosquito cells remain unknown.

Like proliferating cells, viruses require sufficient nutrients to satisfy the metabolic needs of replication (Thai, Graham et al. 2014) (Munger, Bennett et al. 2008). Lack of sufficient nutrients can have adverse effects, including energetic stress and cell death. Diverse viruses rewire the metabolism of infected host cells to meet the biosynthetic needs of virus replication, and our group and others have shown that modulating host cell metabolism can alter virus replication (Thai, Graham et al. 2014, Thai, Thaker et al. 2015, Sanchez, Pulliam et al. 2017). Currently, whether and how ZIKV alters host cell metabolism during infection is unknown. Here, we characterize ZIKV reprogramming of host cell glucose metabolism in both human and C6/36 mosquito cells. We show that the differential effects on nucleotide levels during infection of human versus C6/36 mosquito cells selectively leads to activation of AMPK signaling and contributes to cell death observed in human but not C6/36 mosquito cells during ZIKV infection.

## RESULTS

### Zika virus infection alters glucose consumption in human foreskin fibroblasts.

To determine whether Zika virus infection leads to changes in glucose metabolism, we infected a non-transformed human foreskin fibroblast cell line (HFF-1) with ZIKV strain PRVABC-59 and measured changes in glucose consumption and lactate production by host cells at different time points following infection. HFF-1 cells were used because they have been shown to be permissive to ZIKV infection, and ZIKV has been found to replicate in cells of the male reproductive tract (Hamel, Dejarnac et al. 2015). ZIKV infection of HFF-1 cells significantly increases glucose consumption of infected cells compared to mock-infected cells 1.5 to 2-fold at 24, 36, and 48 hours post-infection. ZIKV-infection of HFF-1 cells also increases the relative lactate production of infected cells relative to mock cells at 36 and 48 hours post-infection (Figure 1A). These findings suggest that ZIKV infection promotes increased glucose utilization and glycolysis in host cells. Infection of HFF-1 cells with UV-inactivated ZIKV does not induce the same increases in glucose consumption and lactate production, indicating that the observed metabolic changes are due to active reprogramming by the virus and not the host cell response to the virus (Figure S1A).

To characterize ZIKV-induced changes in glucose metabolism during infection, HFF-1 cells were labelled with U-$^{13}C_6$-glucose and mock-infected or infected with ZIKV for 18, 24, and 36 hours. Extracted intracellular metabolites and U-$^{13}C_6$-glucose incorporation into different metabolites were measured and analyzed by liquid chromatography mass spectrometry (LC-MS). ZIKV infection increases fractional U-$^{13}C_6$-glucose incorporation into certain glycolytic intermediates compared to mock-infected cells (Figure S1B). Notably, ZIKV infection robustly increases fractional contribution of U-$^{13}C_6$-glucose into nearly all TCA cycle intermediates at all time points post-ZIKV infection compared to mock-infected cells (Figure 1B). Additionally, ZIKV infection generally promotes increased U-$^{13}C_6$-glucose incorporation into different amino acids at 18, 24, and 36 hours post-ZIKV infection (Figure 1C). Taken together, these data suggest that ZIKV infection of human foreskin fibroblast cells promotes increased glucose utilization in the TCA cycle and for amino acid generation.

### Zika virus infection differentially impacts survival and glucose metabolism of human versus C6/36 mosquito cells.

ZIKV is primarily transmitted by *Aedes* species of mosquitoes (Ciota, Bialosuknia et al. 2017) (Grard, Caron et al. 2014). Therefore, we assessed ZIKV infection of *Aedes albopictus* mosquito (C6/36) cells as compared with infection of HFF-1 human cells. ZIKV effectively infects both human HFF-1 cells and C6/36 cells, as can be visualized by flavivirus envelope protein immunostaining (Figure 2A). ZIKV infection of HFF-1 cells leads to increased cell death and decreased number of cells over a period of 48 hours, as visualized by reduced DAPI staining at later time points (Figure 2A). In contrast, ZIKV effectively infects C6/36 cells without promoting cell death or decreasing cell number, as visualized by little change in DAPI staining over 48 hours (Figure 2A). To better characterize ZIKV replication in both cell types, cell-free supernatant was harvested from infected HFF-1 and C6/36 cells and virus titers were determined and quantified. ZIKV infection of both HFF-1 and C6/36 cells leads to increased viral titers from 6 to 30 hours

post-infection. However, after 30 hours, infected HFF-1 cells have decreased viral titer levels compared to earlier time points due to increased cell death, whereas the viral titers of infected C6/36 cells continues to elevate with increasing time points (Figure 2B). Our findings that Zika virus infection promotes death of cultured HFF-1 but not C6/36 cells are similar to previous studies showing that Sindbis virus promotes cell death of mammalian cells but maintains persistent, non-lytic viral replication in mosquito cells (Karpf and Brown 1998) (O'Neill, Olson et al. 2015).

In order to better understand the differences in ZIKV replication in human and mosquito cells, we examined whether there were underlying metabolic differences between ZIKV infection of HFF-1 versus C6/36 cells. We again labeled both HFF-1 and C6/36 cells with U-$^{13}C_6$-glucose and determined relative levels of and glucose incorporation into different metabolites. ZIKV infection of C6/36 mosquito cells significantly elevates glucose contribution to glycolytic intermediates 24 hours post-infection (Figure 2C). In contrast to infection of HFF-1 cells, ZIKV infection of C6/36 cells trends towards decreased glucose contribution to TCA cycle intermediates (Figure 2D). Additionally, glucose contribution to pentose phosphate pathway intermediates increases during ZIKV infection of C6/36 cells 24 hours post-infection (Figure 2E). In contrast, ZIKV infection of HFF-1 cells leads either to no change or decreased glucose incorporation into pentose phosphate pathway intermediates at 24 hours post-infection (Figure 2F). Overall, ZIKV infection of C6/36 mosquito cells increases glucose contribution to glycolytic and pentose phosphate intermediates and decreases glucose contribution to TCA cycle intermediates, whereas infection of human HFF-1 cells promotes increased glucose contribution to TCA cycle intermediates and amino acids and decreased contribution to nucleotides (Figure 2G). These findings suggest that Zika virus promotes differential glucose utilization in human versus C6/36 mosquito cells.

## Zika virus infection selectively depletes nucleotide triphosphate levels in human but not C6/36 mosquito cells.

Since we observed decreased glucose incorporation into pentose phosphate pathway intermediates in ZIKV-infected HFF-1 cells but not in C6/36 cells, we examined whether ZIKV infection leads to different nucleotide levels in human versus C6/36 mosquito cells. ZIKV infection of HFF-1 cells results in increased relative levels of nucleotide mono- and diphosphates but selective depletion of the relative amounts of nucleotide triphosphate levels, particularly ATP and UTP, 24 and 36 hours following infection (Figure 3A, left). Conversely, ZIKV infection of C6/36 cells leads to increased relative levels of most nucleotide mono-, di- and triphosphates at 24 hours post-infection and decreased relative amounts of all nucleotides at 36 hours post-infection (Figure 3A, right). Because of the decrease in relative amounts of ATP and increased levels of ADP and AMP, ZIKV infection of HFF-1 cells leads to robustly elevated ADP/ATP and AMP/ATP ratios at 24 and 36 hours post-infection (Figure 3B). In contrast, ZIKV infection of C6/36 cells does not lead to a significant increase in the AMP/ATP ratio at 24 or 36 hours post-infection and results in only a minor increase in the ADP/ATP ratio at 36 hours post-infection (Figure 3C).

Since we observed a robust increase in the AMP/ATP and ADP/ATP ratios during ZIKV infection of HFF-1 cells, we hypothesized that this imbalance in AMP, ADP, and ATP levels

may activate the serine/threonine kinase AMP-activated protein kinase (AMPK), a major sensor of energetic stress in cells (Mihaylova and Shaw 2011). Consistently, ZIKV infection of HFF-1 cells leads to increased AMPK phosphorylation at Thr172 and elevation of the pAMPK/AMPK ratios at 24 and 36 hours post-infection (Figure 3D, left). Phosphorylation of a well-known target of AMPK signaling, pACC (Ser79) (Mihaylova and Shaw 2011), is also elevated at the same time points post-infection (Figure S2A). ZIKV has previously been shown to promote caspase-mediated cell death of human fetal neuronal progenitor cells and mouse models of ZIKV infection (Hanners, Eitson et al. 2016) (Rosenfeld, Doobin et al. 2017) (Huang, Abraham et al. 2016). Consistently, we observe that ZIKV infection of HFF-1 cells leads to increased cleaved caspase 3 levels 36 hours post-infection (Figure 3D).

Since ZIKV infection of HFF-1 cells depletes nucleotide triphosphate levels, we next assessed whether addition of exogenous nucleotide precursors could at least in part rescue pAMPK/AMPK levels and the cell death phenotype observed. Since ATP and UTP were most significantly depleted, we supplemented media with 250 μM adenine and uridine during ZIKV infection and assessed effects on the pAMPK/AMPK ratio and cleaved caspase 3 levels. Adenine and uridine were added instead of ATP and UTP, since the latter are large, polar molecules that may not readily cross the plasma membrane, and purines are typically salvaged through the base (e.g. adenine) whereas pyrimidines are typically salvaged through the nucleoside (e.g. uridine). Compared to ZIKV-infected cells in regular media, infected cells in the adenine and uridine-supplemented media have reduced pAMPK/AMPK levels (Figure 3D). Interestingly, addition of 250 μM adenine and uridine also reduces levels of caspase 3 cleavage in ZIKV-infected cells 36 hours post-infection compared to cells cultured in regular media (Figure 3D). Importantly, adenine and uridine supplementation of HFF-1 cells during ZIKV infection partially rescues the decrease in relative cell number of ZIKV-infected/mock-infected cells, indicating less cell death during infection with addition of nucleotide precursors (Figure 3E). The relative increase in cell number of infected adenine and uridine supplemented cells relative to cells infected in regular media can also be observed clearly via light microscopy images (Figure S2B). These results suggest that supplementation of exogenous nucleotide precursors can reduce the pAMPK/AMPK ratio and partially rescue caspase-mediated cell death during ZIKV infection.

## Zika virus infection increases AMPK phosphorylation and contributes to Zika virus-induced cell death in clinically relevant models.

We next wanted to determine whether ZIKV infection of other clinically relevant cell types and models results in similar changes in AMPK phosphorylation. Mice lacking the type I interferon (IFN) receptor (IFNAR) have been shown to be permissive to ZIKV infection and viral replication within the central nervous system, testis, uterus, and retina (Jurado, Yockey et al. 2018). We subcutaneously inoculated *Ifnar1*$^{-/-}$ mice with ZIKV ($1\times10^6$ pfu/mouse) and assessed pAMPK levels in the brain 7 days post-infection using immunohistochemistry (IHC). Serial sections of mock-infected mouse brain tissue are negative for ZIKV envelope protein (ENV) and have low levels of pAMPK immunostaining (Figure 4A). ZIKV-infected mouse brain tissue stains positive for ZIKV ENV and displays elevated AMPK phosphorylation compared to mock-infected tissue as quantified across serial mouse brain tissue sections (Figure 4A).

ZIKV infection has also been linked to congenital ocular defects, including retinal abnormalities (de Paula Freitas, de Oliveira Dias et al. 2016). To determine whether similar activation of AMPK occurs in clinically relevant human fetal retinal pigment epithelial (hFRPE) cells, we infected the cells with ZIKV and observed co-localization of the flavivirus envelope protein and pAMPK in ZIKV-infected cells (Figure 4B, bottom). Mock-infected hFRPE cells are negative for the flavivirus envelope protein and have low levels of pAMPK staining (Figure 4B, top). ZIKV-infection of hFRPE cells at MOIs of 1, 5, and 10 leads to increasing pAMPK/AMPK ratios in a dose-dependent manner (Figure 4C). To determine whether there is a link between AMPK activation and caspase-mediated cell death in hFRPE cells, we treated mock-infected and ZIKV-infected cells with and without Compound C, a potent AMPK inhibitor, and measured cleaved caspase 3/7 activity. Compared to mock-infected cells, hFRPE cells infected with ZIKV for 48 hours show increased relative levels of cleaved caspase 3/7 activity (Figure 4D), consistent with the increased cleaved caspase 3 protein levels observed in ZIKV-infected HFF-1 cells (Figure 3D). Interestingly, treatment of ZIKV-infected hFRPE cells with 1 μM Compound C partially rescues the increased cleaved caspase 3/7 activity seen in DMSO-treated ZIKV-infected cells and 5 μM Compound C restores caspase 3/7 activity to levels seen in mock-infected cells (Figure 4D). These data suggest that AMPK is activated by ZIKV infection of human fetal retinal pigment epithelial cells and that blocking AMPK activation can decrease ZIKV-promoted cleaved caspase 3/7 activity.

Our data suggests that AMPK activation contributes to caspase-mediated cell death of ZIKV-infected human cells. In contrast, our data shows that ZIKV-infected C6/36 mosquito cells do not display robustly elevated AMP/ATP and ADP/ATP ratios, and therefore presumably do not have AMPK activation. Therefore, we wanted to determine whether increasing AMPK activity in ZIKV-infected C6/36 cells would be sufficient to promote apoptosis and decrease cell number and viability. We therefore treated C6/36 cells with water or AICAR (5-Aminoimidazole-4-carboxamide ribonucleotide), an adenosine analog and AMPK activator (Garcia and Shaw 2017), and measured cleaved caspase 3/7 activity and cell viability in mock- and ZIKV-infected cells. ZIKV infection of C6/36 cells over 48 hours leads to no change in cleaved caspase activity (Figure 4E), no change in cell viability (Figure 4F), and little visible change in cell number by light microscopy compared to mock-infected cells (Figure 4G). Conversely, AICAR treatment of C6/36 cells is sufficient to increase cleaved caspase 3/7 activity (Figure 4E) and decrease cell viability compared to water-treated, mock-infected cells (Figure 4F). Furthermore, AICAR treatment of ZIKV-infected C6/36 cells over a period of 48 hours post-infection greatly increases cleaved caspase 3/7 activity, decreases cell number and reduces cell viability compared to mock-infected, ZIKV-infected, and mock-infected plus AICAR treated cells (Figures 4E–G). Consistently, we found that pentose phosphate pathway inhibition in ZIKV-infected C6/36 mosquito cells, through dehydroepiandrosterone (DHEA)-mediated inhibition of glucose-6-phosphate dehydrogenase (G6PD) (Figure S3A), also increases cleaved caspase 3/7 activity (Figure S3B). Taken together, these results suggest that differences in pentose phosphate pathway activity and AMPK activation in ZIKV-infected human versus C6/36 mosquito cells may in part underlie the differences in cell death during infection.

## DISCUSSION

This study is the first to characterize metabolic reprogramming during Zika virus infection and to reveal differences between ZIKV-promoted metabolic changes in human versus C6/36 mosquito cells. We show that ZIKV infection differentially promotes altered glucose utilization in human foreskin fibroblasts and C6/36 mosquito cells, with increased glucose utilization in the TCA cycle in human foreskin fibroblasts and increased glucose utilization in the pentose phosphate pathways in C6/36 mosquito cells. We observe selective depletion of nucleotide triphosphates of ZIKV-infected human cells, leading to increased AMP/ATP and ADP/ATP ratios and AMPK activation, which contributes to the caspase-mediated cell death of human cells during infection. Consistently, we show that AMPK phosphorylation is elevated in the brain tissue from a mouse model of ZIKV infection and in clinically relevant human fetal retinal pigment epithelial cells. We also demonstrate that modulation of AMPK activity through supplementation of nucleotide precursors in human cells or pharmacological approaches in both human cells and C6/36 mosquito cells can influence whether or not cells undergo cell death during ZIKV infection.

Though previous studies have identified metabolic changes triggered by infection of other flaviviruses, ZIKV rewiring of glucose metabolism has not yet been elucidated. Another member of the *Flaviviridae* family, Dengue virus (DENV), has been shown to increase glucose consumption and GAPDH activity during infection (Fontaine, Sanchez et al. 2015) (Allonso, Andrade et al. 2015). Hepatitis C virus, a hepacivirus in the *Flaviviridae* family, has been shown to increase pyruvate dehydrogenase kinase (PDK) and hexokinase activity and increase glycolysis and fatty acid synthesis in infected cells (Jung, Jeon et al. 2016) (Ramiere, Rodriguez et al. 2014) (Diamond, Syder et al. 2010) (Waris, Felmlee et al. 2007) (Yang, Hood et al. 2008). However, many studies examining viral metabolic reprogramming have not examined how glucose utilization is altered during infection through metabolic tracer analysis. It is intriguing that while ZIKV infection of both HFF-1 and C6/36 cells promotes glycolysis, infection of human cells leads to increased glucose utilization to generate TCA cycle intermediates rather than pentose phosphate pathway intermediates for nucleotide synthesis. This contrasts with infection of human cells by several other viruses, including adenovirus and human cytomegalovirus (HCMV), which increase glucose utilization towards pentose phosphate pathway intermediates (Vastag, Koyuncu et al. 2011, Thai, Graham et al. 2014). Perhaps one explanation for this difference is that double-stranded DNA viruses, like adenovirus and HCMV, require higher nucleotide generation to synthesize their larger viral genomes, which are approximately 36 kilobases (kb) and 236 kb, respectively, compared to the single-stranded ZIKV RNA genome which is only about 10.8 kb (Russell 2009) (Dolan, Cunningham et al. 2004) (Cunha, Esposito et al. 2016).

The mechanism by which Zika virus can modulate glycolysis and nucleotide levels in infected cells also remains to be determined. A previous study performed with Dengue virus showed that viral NS1 protein can modulate glycolysis by directly interacting with and increasing activity of the enzyme GAPDH (glyceraldehyde-3-phosphate dehydrogenase) (Allonso, Andrade et al. 2015). The ZIKV NS1 protein shares 51–53% homology with DENV NS1 protein (Balmaseda, Stettler et al. 2017). Whether ZIKV NS1 protein or another ZIKV protein can mediate the glycolytic changes observed during infection would provide

insight into the precise molecular mechanism by which ZIKV can alter metabolism of host cells.

To our knowledge, no other study has shown that the underlying metabolic differences between infection of mosquito cells and human cells may in part explain differences in cell death. Here we show that relative levels of nucleotides are differentially altered during ZIKV infection of human and C6/36 mosquito cells, leading to elevation of AMP/ATP ratios, subsequent activation of AMPK, and caspase-mediated cell death in human cells but not mosquito cells. Previous studies have shown modulation of AMPK signaling in human cells during infection with other viruses. However, the role of AMPK signaling during virus infection seems to vary depending on the virus; AMPK activation has been shown by previous studies to exert both antiviral effects, as during infection by West Nile and Rift Valley Fever viruses (Jimenez de Oya, Blazquez et al. 2018) (Moser, Schieffer et al. 2012), and proviral effects for DENV, HCMV, Vaccinia virus, and others [26] (McArdle, Moorman et al. 2012) (Terry, Vastag et al. 2012) (Moser, Jones et al. 2010). Perhaps one advantage of cell death in human cells during lytic virus infection is to prevent propagation of the virus (Upton and Chan 2014) (Everett and McFadden 1999), despite causing pathogenic consequences in some tissues. Infection of mammalian cell lines and mouse models by other flaviviruses has also been shown to induce caspase 3 cleavage. West Nile virus infection promotes caspase activation in human glioblastoma cells and mouse brain tissue (Kleinschmidt, Michaelis et al. 2007) (Samuel, Morrey et al. 2007), and Japanese encephalitis virus infection promotes caspase 3 cleavage in both human medulloblastoma and mouse neuroblastoma cells (Tsao, Su et al. 2008) (Yang, Shiu et al. 2009). However, these studies have not explored in detail the upstream causes of caspase 3 activation, and it will be interesting for future studies to explore whether altered nucleotide levels and AMPK activation lead to apoptosis during infection by these and other flaviviruses.

Our study describes key metabolic differences between ZIKV infection of human and C6/36 mosquito cells, provides a link between AMPK activation and cell death during infection, and sets the stage for further studies to examine whether metabolic reprogramming plays a role in the vector supporting ZIKV replication without impaired health *in vivo*.

## LIMITATIONS OF THE STUDY

We show ZIKV-induced metabolic rewiring of multiple human cell lines and ZIKV-induced promotion of AMPK phosphorylation in human cells *in vitro* and mouse brain tissue *in vivo*. However, since our findings on ZIKV-induced metabolic rewiring of mosquito cells were derived from only one mosquito cell line, they may not be reflective of the metabolic changes conferred by ZIKV at the organismal level in mosquitoes. Studies in mosquitoes is currently limited due to limited availability of mosquito cell lines, particularly those that are permissive to ZIKV replication. Additionally, since *in vivo* tissue metabolism varies greatly from *in vitro* cell culture conditions, future studies should determine metabolic changes conferred by Zika infection in *in vivo* models of different species.

# STAR METHODS

## CONTACT FOR REAGENT AND RESOURCE SHARING

Further information and requests for resources and reagents should be directed to and will be fulfilled by the Lead Contact, Heather Christofk (hchristofk@mednet.ucla.edu).

## EXPERIMENTAL MODEL AND SUBJECT DETAILS

Vero, Human foreskin fibroblast (HFF-1), *Aedes albopictus* C6/36, and Aedes cells were obtained from the ATCC and cultured in DMEM high glucose medium supplemented with 10% fetal bovine serum and 1% penicillin/streptomycin. Vero and HFF-1 cells were maintained at 37°C with 5% $CO_2$, while C6/36 cells were maintained at 28°C with 5% $CO_2$. Human fetal retinal pigment epithelial (FRPE) cells were kindly provided by Dr. Guoping Fan at UCLA with required informed consent described in previously published reports (Liao, Yu et al. 2010) (Liu, Jiang et al. 2014). Use of this established hFRPE line for the study was approved by the Cedars-Sinai Medical Center Institutional Biosafety Committee (IBC). hFRPE cells were grown in DMEM high glucose medium supplemented with 10% fetal bovine serum and 1% penicillin/streptomycin. FRPEs were originally isolated from fetal retina (~20-week-old) using a previously published protocol (Sonoda, Spee et al. 2009) and were incubated at 37°C with 5% $CO_2$. Since the hFRPE line is deidentified, information on the sex of the line is unavailable.

**Mice—**All animal experiements in the study were approved by the Institutional Animal Care and Use Committee (IACUC). 4–6 week old male *Ifnar1*−/− (A129 or IFN-αβR-KO; strain: B6.129S2-Ifnar1tm1Agt) mice (Jackson Laboratory) were used for the *in vivo* ZIKV infection experiments. Mice were housed at Cedars-Sinai Medical Center Vivarium at 37°C with 12 hour light/dark cycles and fed autoclaved rodent chow.

## METHOD DETAILS

**Zika Virus Generation and Plaque Assay—**Zika virus (ZIKV) Puerto Rico strain PRVABC-59 (GenBank number KU501215) was obtained through distribution from the United States Center for Disease Control and Prevention (CDC). Virus stocks were produced by collecting cell-free supernatant from infected C6/36 cell culture 6 days after infection at a multiplicity of infection (MOI) of 0.01. Virus titers were determined in duplicate by plaque assay in Vero cells as described previously (Gong, Zhang et al. 2018). Briefly, 60,000 Vero cells were seeded in 12-well plates 24 hours before infection, then infected with ZIKV for 1 h with gentle shaking every 15 min and overlaid with 1% methylcellulose (Sigma). Four days later, cells were fixed and stained with 1% crystal violet in 20% ethanol, and plaques were counted to determine the titer.

**Zika virus infection of HFF-1, C6/36, or FRPE cells—**HFF-1, C6/36, or FRPE cells were seeded at subconfluency prior to ZIKV infection. After 24-hours, ZIKV inoculum, with a multiplicity of infection of 1 (for FRPE cells) or 3 (for HFF-1 and C6/36 cells), was formulated using the base media specified for each cell type. A total of 1 ml of viral inoculum was added to each well and the plates were incubated at 37 °C with 5% $CO_2$ for 2–4 hours. After the incubation period, the base media was replaced with complete media at

a volume of 3 mL per well. For the uninfected (mock) group, each cell type received the specified cell-growth media that was concurrently used to prepare the viral inoculum, as described above. At the end of each timepoint, cell lysates and RNA were harvested for downstream analyses.

**Measurement of Glucose Consumption Rates and Lactate Production Rates—** Cellular glucose consumption and lactate production rates were measured using a Nova Biomedical BioProfile Basic Analyzer. Briefly, cells were seeded in triplicate in 6-well plates at 50% confluency to ensure that the measurements would be taken when the cells were subconfluent. Twenty-four hours post-seeding, the media was refreshed for all cells and cells were either mock-infected or infected with ZIKV at an MOI of 3. Media was also added to empty wells as a blank control. After the indicated duration of infection, 1 mL of media was removed from each sample and the blank control, and media samples were analyzed in the Nova BioProfile Basic Analyzer. Cell numbers were determined using a Beckman Coulter particle analyzer and used to normalize the calculated rates.

**Intracellular metabolite extraction and analysis—**Cells were seeded in six-well plates, infected with ZIKV at a MOI of 3 for the listed duration of time, and metabolites were extracted at 70–80% confluence. Medium was replaced with medium containing the U-$^{13}C_6$-glucose at the time of infection. Cells were washed with ice-cold 150 mM ammonium acetate (pH 7.3) and scraped off the plate in 800 µl ice-cold 50% methanol. 10 nmol norvaline was added as an internal standard, followed by 400 µl chloroform. Following vigorous vortexing, samples were centrifuged at maximum speed, the aqueous layer was transferred to a glass vial and the metabolites were dried under an EZ-2Elite evaporator. Metabolites were resuspended in 50 µl 70% acetonitrile (ACN) and 5 µl of this solution used for the mass spectrometer-based analysis. The analysis was performed on a Q Exactive (Thermo Scientific) in polarity-switching mode with positive voltage 4.0 kV and negative voltage 4.0 kV. The mass spectrometer was coupled to an UltiMate 3000RSLC (Thermo Scientific) UHPLC system. Mobile phase A was 5 mM $NH_4AcO$, pH 9.9, B was ACN and the separation achieved on a Luna 3 mm NH2 100 A (150 × 2.0 mm) (Phenomenex) column. The flow was 200 µl $min^{-1}$, and the gradient ran from 15% A to 95% A in 18 min, followed by an isocratic step for 9 min and re-equilibration for 7 min. Metabolites were detected and quantified as area under the curve based on retention time and accurate mass (≤3 p.p.m.) using the TraceFinder 3.1 (Thermo Scientific) software. Relative amounts of metabolites between various conditions, as well as percentage of labelling, were calculated and corrected for naturally occurring $^{13}C$ abundance.

**Viral Growth Analysis—**C6/36 or HFF-1 cells were seeded in 12-well plates 24 hours before infection to generate a monolayer of 80% confluence. Cells were inoculated with ZIKV for 1 hour at an MOI of 3 for single step growth analysis. The inoculum was removed, the infected monolayer was rinsed with phosphate-buffered saline (PBS), and fresh medium was replenished. Cell-free virus was collected in the medium at indicated times post-infection, and viral titer was determined by plaque assay.

**Immunofluorescence and Brightfield Imaging—**Intracellular localization of proteins of interest was analyzed by using an immunofluorescence assay. Cells were seeded in 12-well plates 24hr prior to ZIKV infection. At the indicated times post-infection, the cells were washed with PBS, fixed with 4% paraformaldehyde for 20 minutes, permeabilized with 0.1% Triton for 15 minutes, and blocked with 5% fetal bovine serum in PBS at room temperature for 30 min. Cells were incubated with primary antibodies, including Cell Signaling Phospho-AMPKα (Thr172) (40H9) rabbit mAb #2535 (1:100) and EMD Millipore mouse anti-Flavivirus Group Antigen (MAB10216) (1:1000) for 30 minutes at room temperature and subsequently labeled with secondary antibodies coupled to Alexa Fluor 488 (Invitrogen-Molecular Probes). Cells were stained with DAPI for DNA staining and visualized using a Nikon Eclipse Ti Immunofluroscence Microscope with 30 Nikon Intenselight C-HGFI using the 63X/1.40–0.60 oil lens.

**Western Blotting—**Cells were lysed in 50 mM Tris pH 7.4, 1% NP-40, 0.25% sodium deoxycholate, 1 mM EDTA, 150 mM NaCl, 1 mM $Na_3VO_4$, 20 mM NaF, 1mM PMSF, 2 μg $ml^{-1}$ aprotinin, 2 μg $ml^{-1}$ leupeptin and 0.7 μg $ml^{-1}$ pepstatin. Protein concentrations of cell extracts were determined by the Bradford assay. Western blot analysis was carried out as previously described (Thai, Thaker et al. 2015). The following antibodies were used as probes: Actin (Abcam; 1:1000), Phospho-AMPKα Thr172 (Cell Signaling #2535; 1:1000), AMPKα (Cell Signaling #2532; 1:1000), Caspase 3 (Cell Signaling #9662; 1:1000), Cleaved Caspase 3 (Asp175) 5A1E (Cell Signaling #9664; 1:1000), pACC1 (Ser79) D7D11 (Cell Signaling #11818; 1:1000), ACC1 (Cell Signaling #4190; 1:1000).

**Nucleotide Rescue Experiments—**Cells were seeded at subconfluency in 6-well plates. The next day, 200μM of adenine (Sigma A2786) and 200μM of uridine (Sigma U3003) were added to cell media versus an equal volume water-only control concurrently with ZIKV infection at an MOI of 3. After 48 hours incubation period, cell numbers were determined using a Beckman Coulter particle analyzer.

***In vivo* mouse model of ZIKV infection—**4–6-week old *Ifnar1*$^{-/-}$ male mice were inoculated with phosphate buffered saline (PBS) (n=5 mice) or PRVABC ZIKV ($1 \times 10^6$ pfu per mouse in a 40 μl volume) (n=5 mice) by subcutaneous route in the hind limb region under isoflurane anesthesia. Tissues were collected at 7 dpi.

**Compound C Experiments—**An antiviral analysis screen of Dorsomorphin (Compound C) (Abcam) in a dose-response was performed in fetal retinal pigment epithelial cells. RPE cells were seeded at a cell density of $5 \times 10^3$ cells per well in 96-well plates and $10 \times 10^3$ cells per well in 48-well plates. Sixteen hours later, cells were infected with ZIKV at an MOI of 1 or 10 for 1 hour and Compound C was added to cells to a final concentration of 1uM or 5uM. Infected cells were subjected to cell viability and apoptosis assays two days later. RNA was isolated from the same cells for quantification of the ZIKV genome.

**Caspase 3/7 Assay—**Caspase-Glo 3/7 Assay was performed as indicated in the manufacturer's protocol (Promega, USA). Briefly, at the 48 hours post-infection, ZIKV infected and mock-infected FRPE or C6/36 cells were incubated with the pro-luminescent caspase-3/7 substrate for 1 hour at room temperature. Following incubation, 100 μL of lysate

was transferred to a white 96-well microtiter plate and the luminescence signal was read using a luminometer (Glomax Microplate Luminometer, Promega).

**Mouse brain tissue immunohistochemistry—**Brain tissue was incubated in 4% PFA for an hour and transferred to PBS. Tissues were then submerged in 10%, 20%, and 30% sucrose for an hour each. Tissue was then embedded in OCT (Fisher Healthcare) and incubated overnight at −80°C. Tissues were cut (6 μm thick) using a Leica cryostat microtome and mounted on Super Frost microscope slides (VWR). Sections were washed 3 times and permeabilized using blocking buffer (0.3% Triton X-100, 0.1% BSA, in 1 X PBS) for 1 hour at room temperature. For ZIKV staining, sections were incubated overnight at 4°C with a polyclonal anti-ZIKV Envelope protein antibody (rabbit, 1:250) (GeneTex) or anti-Phospho-AMPKα (Thr172) (clone 40H9) (Rabbit, 1:150). The sections were then rinsed with 1X PBS three times and incubated with secondary antibody, Alexa Fluor-conjugated 488 or 555 antibodies (raised in rabbit, 1:1000; or mouse, 1:1000) for 1 hour at room temperature. Nucleus was stained with DAPI (4',6-Diamidino-2-Phenylindole, Dihydrochloride) (Life Technologies) at a dilution of 1:1000 in blocking buffer. Image acquisition was done using the Zeiss LSM 700 confocal microscope. The Zeiss imaging software was used with the maximum intensity projection feature to capture images. Image J's plug-in cell counter feature was used to count the positively stained cells by a double blinded approach. The mean positively-stained cells from 4 independent images were calculated.

**AICAR Experiment—**C6/36 cells were treated with water or 300 μM AICAR (Sigma A9978) dissolved in water and simultaneously mock-infected or infected with ZIKV at an MOI of 3. 48 hours post-infection, cells were collected and cell viability measurements using trypan blue staining or cleaved caspase 3/7 activity were determined. Light microscope images were taken with the Zeiss Axiovert.

### QUANTIFICATION AND AND STATISTICAL ANALYSIS

All numerical data were calculated and plotted with mean +/− s.d. Results were analyzed using Graphpad Prism 8 software. Normality was determined by the Shapiro-Wilk test, followed by unpaired Student's *t*-test for normally distributed data. Multiple group comparisons were made by ANOVA with Student's t-test post-tests used between groups. Differences were considered statistically significant when $p<0.05$ (*) or $p<0.01$ (**) or $p<0.005$ (***). Additional statistical parameters can be found in the figure legends.

## Supplementary Material

Refer to Web version on PubMed Central for supplementary material.

## ACKNOWLEDGMENTS

We thank Dr. Guoping Fan (UCLA) for providing the human fetal retinal pigment epithelial cells used in the experiments. We thank Dr. Laura Martinez for technical assistance. S.K.T. is a pre-doctoral fellow supported by the UCLA Virology and Gene Therapy Training Grant (T32AI060567) and UCLA Tumor Immunology Training Grant (USHHS Ruth L. Kirschstein Institutional National Research Service Award #T32 CA009056). H.R.C. was supported by a Research Scholar Grant, RSG-16-111-01-MPC, from the American Cancer Society, NIH/NCI RO1 CA215185-01, and the UCLA Jonsson Comprehensive Cancer Center and Eli and Edythe Broad Center for

Regenerative Medicine Ablon Scholars Program. V.A. was supported by a California Institute for Regenerative Medicine (CIRM) award DISC2-10188.

## REFERENCES

Allonso D, Andrade IS, Conde JN, Coelho DR, Rocha DC, da Silva ML, Ventura GT, Silva EM and Mohana-Borges R (2015). "Dengue Virus NS1 Protein Modulates Cellular Energy Metabolism by Increasing Glyceraldehyde-3-Phosphate Dehydrogenase Activity." J Virol 89(23): 11871–11883. [PubMed: 26378175]

Balmaseda A, Stettler K, Medialdea-Carrera R, Collado D, Jin X, Zambrana JV, Jaconi S, Cameroni E, Saborio S, Rovida F, Percivalle E, Ijaz S, Dicks S, Ushiro-Lumb I, Barzon L, Siqueira P, Brown DWG, Baldanti F, Tedder R, Zambon M, de Filippis AMB, Harris E and Corti D (2017). "Antibody-based assay discriminates Zika virus infection from other flaviviruses." Proc Natl Acad Sci U S A 114(31): 8384–8389. [PubMed: 28716913]

Baud D, Gubler DJ, Schaub B, Lanteri MC and Musso D (2017). "An update on Zika virus infection." Lancet 390(10107): 2099–2109. [PubMed: 28647173]

Ciota AT, Bialosuknia SM, Ehrbar DJ and Kramer LD (2017). "Vertical Transmission of Zika Virus by Aedes aegypti and Ae. albopictus Mosquitoes." Emerg Infect Dis 23(5): 880–882. [PubMed: 28277199]

Cunha MS, Esposito DL, Rocco IM, Maeda AY, Vasami FG, Nogueira JS, de Souza RP, Suzuki A, Addas-Carvalho M, Mde L. Barjas-Castro, Resende MR, Stucchi RS, Ide F.Boin, Katz G, Angerami RN and da Fonseca BA (2016). "First Complete Genome Sequence of Zika Virus (Flaviviridae, Flavivirus) from an Autochthonous Transmission in Brazil." Genome Announc 4(2).

Daep CA, Munoz-Jordan JL and Eugenin EA (2014). "Flaviviruses, an expanding threat in public health: focus on dengue, West Nile, and Japanese encephalitis virus." J Neurovirol 20(6): 539–560. [PubMed: 25287260]

de Oliveira WK, Carmo EH, Henriques CM, Coelho G, Vazquez E, Cortez-Escalante J, Molina J, Aldighieri S, Espinal MA and Dye C (2017). "Zika Virus Infection and Associated Neurologic Disorders in Brazil." N Engl J Med 376(16): 1591–1593. [PubMed: 28402236]

de Paula Freitas B, de Oliveira Dias JR, Prazeres J, Sacramento GA, Ko AI, Maia M and Belfort R Jr. (2016). "Ocular Findings in Infants With Microcephaly Associated With Presumed Zika Virus Congenital Infection in Salvador, Brazil." JAMA Ophthalmol.

Diamond DL, Syder AJ, Jacobs JM, Sorensen CM, Walters KA, Proll SC, McDermott JE, Gritsenko MA, Zhang Q, Zhao R, Metz TO, Camp DG 2nd, Waters KM, Smith RD, Rice CMand Katze MG(2010). "Temporal proteome and lipidome profiles reveal hepatitis C virus-associated reprogramming of hepatocellular metabolism and bioenergetics." PLoS Pathog 6(1): e1000719.

Dolan A, Cunningham C, Hector RD, Hassan-Walker AF, Lee L, Addison C, Dargan DJ, McGeoch DJ, Gatherer D, Emery VC, Griffiths PD, Sinzger C, McSharry BP, Wilkinson GW and Davison AJ (2004). "Genetic content of wild-type human cytomegalovirus." J Gen Virol 85(Pt 5): 1301–1312. [PubMed: 15105547]

Everett H and McFadden G (1999). "Apoptosis: an innate immune response to virus infection." Trends Microbiol 7(4): 160–165. [PubMed: 10217831]

Fontaine KA, Sanchez EL, Camarda R and Lagunoff M (2015). "Dengue virus induces and requires glycolysis for optimal replication." J Virol 89(4): 2358–2366. [PubMed: 25505078]

Garcia D and Shaw RJ (2017). "AMPK: Mechanisms of Cellular Energy Sensing and Restoration of Metabolic Balance." Mol Cell 66(6): 789–800. [PubMed: 28622524]

Gong D, Zhang T-H, Zhao D, Du Y, Chapa TJ, Shi Y, Wang L, Contreras D, Zeng G, Shi P-Y, Wu T-T, Arumugaswami V and Sun R (2018). "High-Throughput Fitness Profiling of Zika Virus E Protein Reveals Different Roles for Glycosylation during Infection of Mammalian and Mosquito Cells." iScience 1: 97–111. [PubMed: 30227960]

Grard G, Caron M, Mombo IM, Nkoghe D, Mboui Ondo S, Jiolle D, Fontenille D, Paupy C and Leroy EM (2014). "Zika virus in Gabon (Central Africa)−−2007: a new threat from Aedes albopictus?" PLoS Negl Trop Dis 8(2): e2681.

Hamel R, Dejarnac O, Wichit S, Ekchariyawat P, Neyret A, Luplertlop N, Perera-Lecoin M, Surasombatpattana P, Talignani L, Thomas F, Cao-Lormeau VM, Choumet V, Briant L, Despres P,

Amara A, Yssel H and Misse D (2015). “Biology of Zika Virus Infection in Human Skin Cells.” J Virol 89(17): 8880–8896. [PubMed: 26085147]

Hanners NW, Eitson JL, Usui N, Richardson RB, Wexler EM, Konopka G and Schoggins JW (2016). “Western Zika Virus in Human Fetal Neural Progenitors Persists Long Term with Partial Cytopathic and Limited Immunogenic Effects.” Cell Rep 15(11): 2315–2322. [PubMed: 27268504]

Huang WC, Abraham R, Shim BS, Choe H and Page DT (2016). “Zika virus infection during the period of maximal brain growth causes microcephaly and corticospinal neuron apoptosis in wild type mice.” Sci Rep 6: 34793. [PubMed: 27713505]

Jimenez de Oya N, Blazquez AB, Casas J, Saiz JC and Acebes M. A. Martin (2018). “Direct Activation of Adenosine Monophosphate-Activated Protein Kinase (AMPK) by PF-06409577 Inhibits Flavivirus Infection through Modification of Host-Cell Lipid Metabolism. ” Antimicrob Agents Chemother.

Jung GS, Jeon JH, Choi YK, Jang SY, Park SY, Kim SW, Byun JK, Kim MK, Lee S, Shin EC, Lee IK, Kang YN and Park KG (2016). “Pyruvate dehydrogenase kinase regulates hepatitis C virus replication.” Sci Rep 6: 30846. [PubMed: 27471054]

Jurado KA, Yockey LJ, Wong PW, Lee S, Huttner AJ and Iwasaki A (2018). “Antiviral CD8 T cells induce Zika-virus-associated paralysis in mice.” Nat Microbiol 3(2): 141–147. [PubMed: 29158604]

Karpf AR and Brown DT (1998). “Comparison of Sindbis virus-induced pathology in mosquito and vertebrate cell cultures.” Virology 240(2): 193–201. [PubMed: 9454692]

Kleinschmidt MC, Michaelis M, Ogbomo H, Doerr HW and Cinatl J Jr. (2007). “Inhibition of apoptosis prevents West Nile virus induced cell death.” BMC Microbiol 7: 49. [PubMed: 17535425]

Liang Q, Luo Z, Zeng J, Chen W, Foo SS, Lee SA, Ge J, Wang S, Goldman SA, Zlokovic BV, Zhao Z and Jung JU (2016). “Zika Virus NS4A and NS4B Proteins Deregulate Akt-mTOR Signaling in Human Fetal Neural Stem Cells to Inhibit Neurogenesis and Induce Autophagy.” Cell Stem Cell 19(5): 663–671. [PubMed: 27524440]

Liao JL, Yu J, Huang K, Hu J, Diemer T, Ma Z, Dvash T, Yang XJ, Travis GH, Williams DS, Bok D and Fan G (2010). “Molecular signature of primary retinal pigment epithelium and stem-cell-derived RPE cells.” Hum Mol Genet 19(21): 4229–4238. [PubMed: 20709808]

Liu Z, Jiang R, Yuan S, Wang N, Feng Y, Hu G, Zhu X, Huang K, Ma J, Xu G, Liu Q, Xue Z and Fan G (2014). “Integrated analysis of DNA methylation and RNA transcriptome during in vitro differentiation of human pluripotent stem cells into retinal pigment epithelial cells.” PLoS One 9(3): e91416.

McArdle J, Moorman NJ and Munger J (2012). “HCMV targets the metabolic stress response through activation of AMPK whose activity is important for viral replication.” PLoS Pathog 8(1): e1002502.

Mihaylova MM and Shaw RJ (2011). “The AMPK signalling pathway coordinates cell growth, autophagy and metabolism.” Nat Cell Biol 13(9): 1016–1023. [PubMed: 21892142]

Miner JJ and Diamond MS (2017). “Zika Virus Pathogenesis and Tissue Tropism.” Cell Host Microbe 21(2): 134–142. [PubMed: 28182948]

Moser TS, Jones RG, Thompson CB, Coyne CB and Cherry S (2010). “A kinome RNAi screen identified AMPK as promoting poxvirus entry through the control of actin dynamics.” PLoS Pathog 6(6): e1000954.

Moser TS, Schieffer D and Cherry S (2012). “AMP-activated kinase restricts Rift Valley fever virus infection by inhibiting fatty acid synthesis.” PLoS Pathog 8(4): e1002661.

Munger J, Bennett BD, Parikh A, Feng XJ, McArdle J, Rabitz HA, Shenk T and Rabinowitz JD (2008). “Systems-level metabolic flux profiling identifies fatty acid synthesis as a target for antiviral therapy.” Nat Biotechnol 26(10): 1179–1186. [PubMed: 18820684]

O’Neill K, Olson BJ, Huang N, Unis D and Clem RJ (2015). “Rapid selection against arbovirus-induced apoptosis during infection of a mosquito vector.” Proc Natl Acad Sci U S A 112(10): E1152–1161. [PubMed: 25713358]

Oh Y, Zhang F, Wang Y, Lee EM, Choi IY, Lim H, Mirakhori F, Li R, Huang L, Xu T, Wu H, Li C, Qin CF, Wen Z, Wu QF, Tang H, Xu Z, Jin P, Song H, Ming GL and Lee G (2017). "Zika virus directly infects peripheral neurons and induces cell death." Nat Neurosci 20(9): 1209–1212. [PubMed: 28758997]

Petersen LR, Jamieson DJ and Honein MA (2016). "Zika Virus." N Engl J Med 375(3): 294–295.

Ramiere C, Rodriguez J, Enache LS, Lotteau V, Andre P and Diaz O (2014). "Activity of hexokinase is increased by its interaction with hepatitis C virus protein NS5A." J Virol 88(6): 3246–3254. [PubMed: 24390321]

Rosenfeld AB, Doobin DJ, Warren AL, Racaniello VR and Vallee RB (2017). "Replication of early and recent Zika virus isolates throughout mouse brain development." Proc Natl Acad Sci U S A 114(46): 12273–12278. [PubMed: 29087938]

Russell WC (2009). "Adenoviruses: update on structure and function." J Gen Virol 90(Pt 1): 1–20. [PubMed: 19088268]

Saiz JC, Vazquez-Calvo A, Blazquez AB, Merino-Ramos T, Escribano-Romero E and Martin-Acebes MA (2016). "Zika Virus: the Latest Newcomer." Front Microbiol 7: 496. [PubMed: 27148186]

Samuel MA, Morrey JD and Diamond MS (2007). "Caspase 3-dependent cell death of neurons contributes to the pathogenesis of West Nile virus encephalitis." J Virol 81(6): 2614–2623. [PubMed: 17192305]

Sanchez EL, Pulliam TH, Dimaio TA, Thalhofer AB, Delgado T and Lagunoff M (2017). "Glycolysis, Glutaminolysis, and Fatty Acid Synthesis Are Required for Distinct Stages of Kaposi's Sarcoma-Associated Herpesvirus Lytic Replication." J Virol 91(10).

Sonoda S, Spee C, Barron E, Ryan SJ, Kannan R and Hinton DR (2009). "A protocol for the culture and differentiation of highly polarized human retinal pigment epithelial cells." Nat Protoc 4(5): 662–673. [PubMed: 19373231]

Tang H, Hammack C, Ogden SC, Wen Z, Qian X, Li Y, Yao B, Shin J, Zhang F, Lee EM, Christian KM, Didier RA, Jin P, Song H and Ming GL (2016). "Zika Virus Infects Human Cortical Neural Progenitors and Attenuates Their Growth." Cell Stem Cell 18(5): 587–590. [PubMed: 26952870]

Terry LJ, Vastag L, Rabinowitz JD and Shenk T (2012). "Human kinome profiling identifies a requirement for AMP-activated protein kinase during human cytomegalovirus infection." Proc Natl Acad Sci U S A 109(8): 3071–3076. [PubMed: 22315427]

Thai M, Graham NA, Braas D, Nehil M, Komisopoulou E, Kurdistani SK, McCormick F, Graeber TG and Christofk HR (2014). "Adenovirus E4ORF1-induced MYC activation promotes host cell anabolic glucose metabolism and virus replication." Cell Metab 19(4): 694–701. [PubMed: 24703700]

Thai M, Thaker SK, Feng J, Du Y, Hu H, Wu T. Ting, Graeber TG, Braas D and Christofk HR (2015). "MYC-induced reprogramming of glutamine catabolism supports optimal virus replication." Nat Commun 6: 8873. [PubMed: 26561297]

Tsao CH, Su HL, Lin YL, Yu HP, Kuo SM, Shen CI, Chen CW and Liao CL (2008). "Japanese encephalitis virus infection activates caspase-8 and −9 in a FADD-independent and mitochondrion-dependent manner." J Gen Virol 89(Pt 8): 1930–1941. [PubMed: 18632964]

Upton JW and Chan FK (2014). "Staying alive: cell death in antiviral immunity." Mol Cell 54(2): 273–280. [PubMed: 24766891]

Vastag L, Koyuncu E, Grady SL, Shenk TE and Rabinowitz JD (2011). "Divergent effects of human cytomegalovirus and herpes simplex virus-1 on cellular metabolism." PLoS Pathog 7(7): e1002124.

Waris G, Felmlee DJ, Negro F and Siddiqui A (2007). "Hepatitis C virus induces proteolytic cleavage of sterol regulatory element binding proteins and stimulates their phosphorylation via oxidative stress." J Virol 81(15): 8122–8130. [PubMed: 17507484]

Yang TC, Shiu SL, Chuang PH, Lin YJ, Wan L, Lan YC and Lin CW (2009). "Japanese encephalitis virus NS2B-NS3 protease induces caspase 3 activation and mitochondria-mediated apoptosis in human medulloblastoma cells." Virus Res 143(1): 77–85. [PubMed: 19463724]

Yang W, Hood BL, Chadwick SL, Liu S, Watkins SC, Luo G, Conrads TP and Wang T (2008). "Fatty acid synthase is up-regulated during hepatitis C virus infection and regulates hepatitis C virus entry and production." Hepatology 48(5): 1396–1403. [PubMed: 18830996]

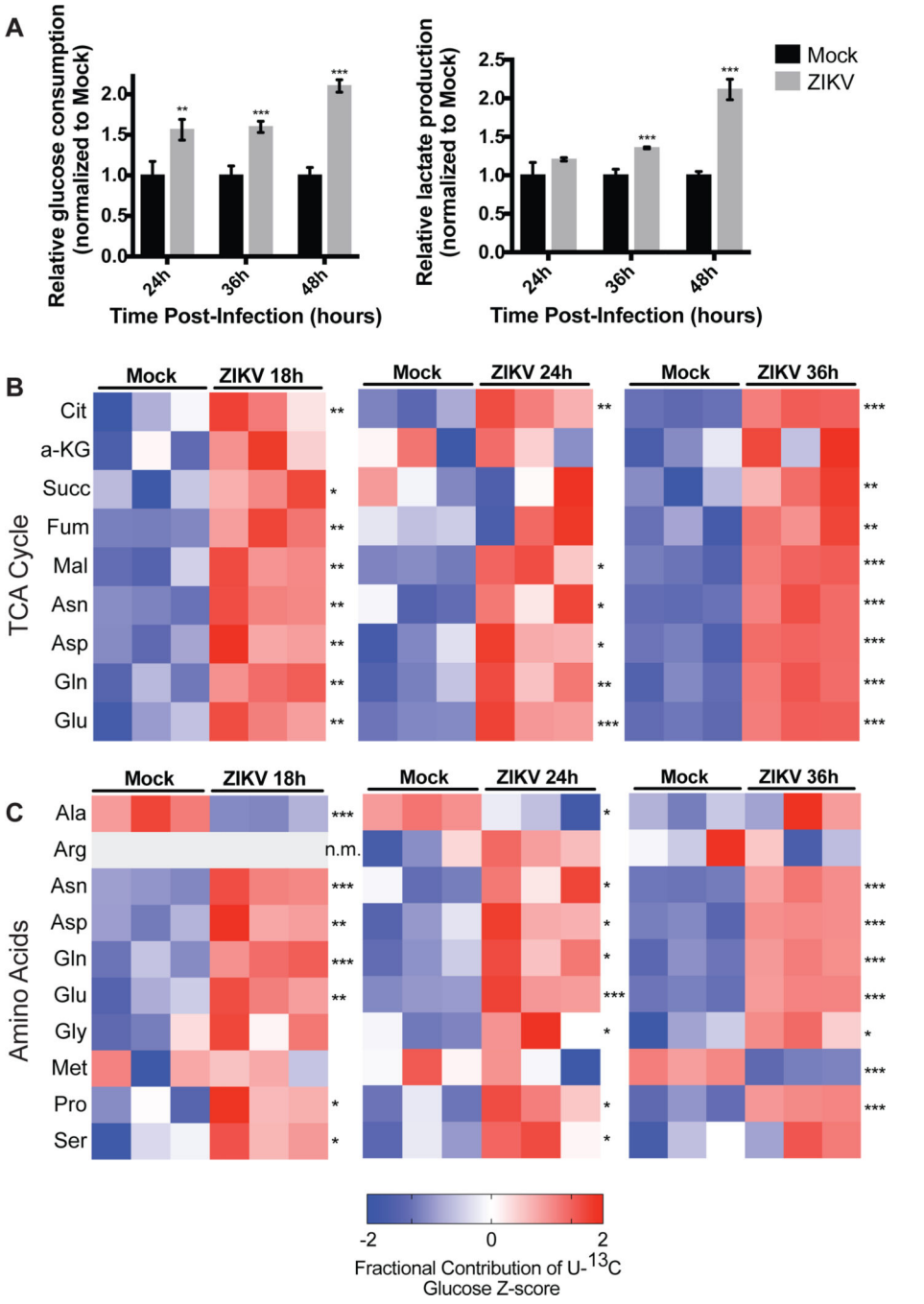


**Figure 1. Zika virus infection alters glucose utilization in human foreskin fibroblasts.**

(A) HFF-1 cells were either mock-infected or infected by ZIKV at a MOI of 3, and glucose consumption and lactate production rates of host cells were measured at 24, 36, and 48 hours post-infection. Rates are normalized relative to mock-infected cells. Data are represented as mean +/− s.d. (B) HFF-1 cells were labeled with U-$^{13}$C glucose and metabolites were extracted at 18, 24, and 36 hours post-ZIKV infection and analyzed via LC-MS. Z-scores of the fractional contribution of U-$^{13}C_6$-glucose into TCA cycle intermediates are displayed in the heatmaps. (C) Mock- and ZIKV-infected HFF-1 cells were labeled with U-$^{13}C_6$-glucose

and fractional contribution of glucose into amino acids are quantified by z-scores. *n.m.* indicates that the metabolite was not measured. *p*-values were calculated using Student's *t*-test and error bars indicate s.d. (n=3), **p* < 0.05, ***p* < 0 .01, ****p* < 0.005.

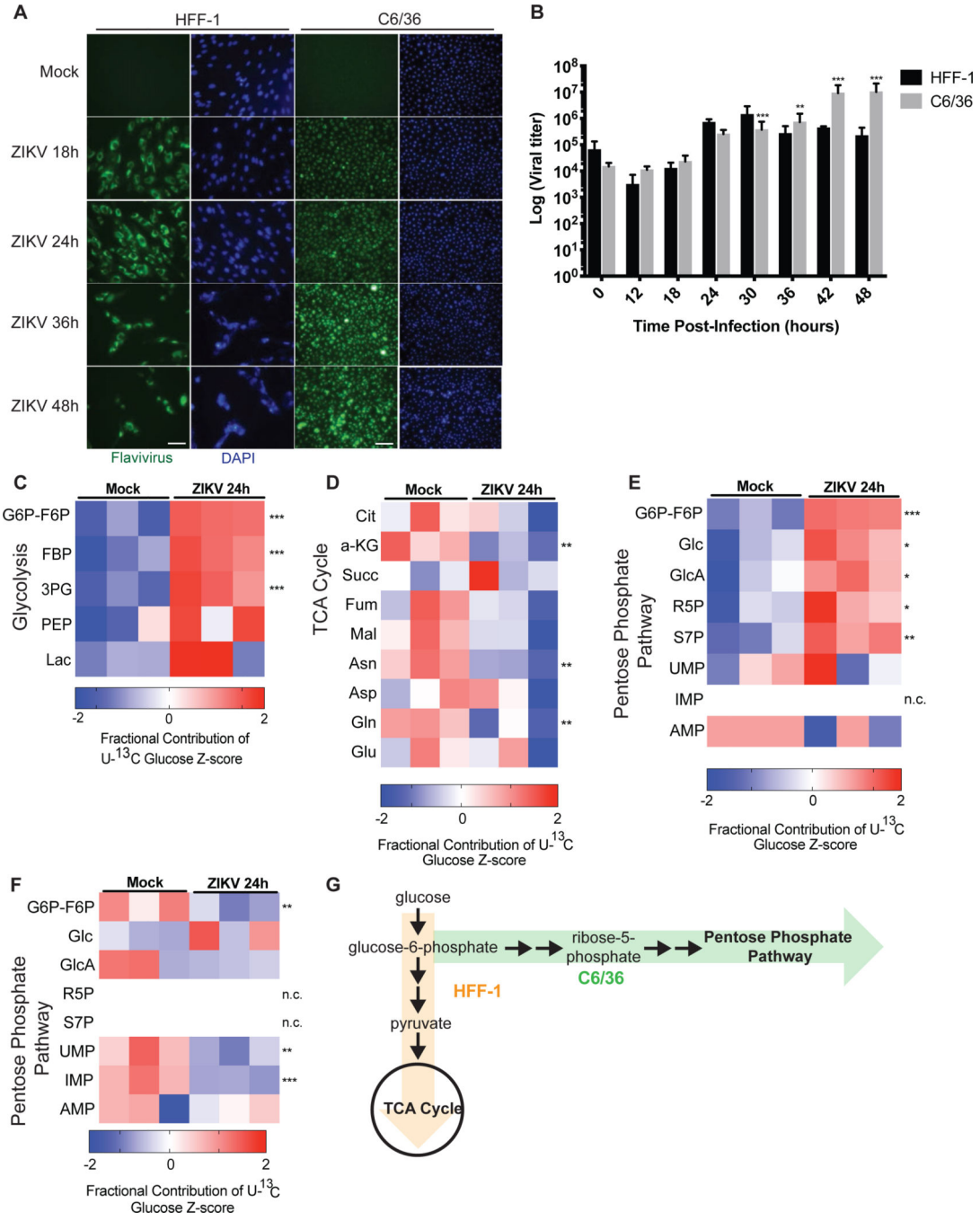


**Figure 2. Zika virus infection differentially impacts survival and glucose metabolism of human versus C6/36 mosquito cells.**

(A) HFF-1 and C6/36 mosquito cells were mock-infected or infected with ZIKV at an MOI of 3 and visualized via immunofluorescence by DAPI staining (blue) and Flavivirus envelope protein staining (green). Scale bar, 20 μM. (B) HFF-1 and C6/36 mosquito cells were infected with ZIKV at an MOI of 3. Cell-free supernatant was collected from infected cultures at indicated times post infection, and virus titers were determined in duplicate by plaque assay in Vero cells (n=4). (C) Mock- and ZIKV-infected C6/36 cells were labeled with U-$^{13}C_6$-glucose for 24 hours and metabolites were extracted and analyzed via LC-MS.

Fractional contribution of labeled glucose into glycolytic intermediates, (D) TCA cycle intermediates, and (E) pentose phosphate pathway intermediates were quantified and displayed as z-scores. (F) HFF-1 cells were labeled with U-$^{13}C_6$-glucose and mock- or ZIKV-infected. Metabolites were extracted and analyzed via LC-MS to determine fractional contribution of glucose to pentose phosphate pathway intermediates. (G) Schematic of glucose metabolite tracing data in HFF-1 (orange) versus C6/36 cells (green). *n.c.* indicates there was no change in fractional contribution between groups measured. *p*-values were calculated using Student's *t*-test and error bars indicate s.d. (n=3), $*p < 0.05$, $**p < 0.01$, $***p < 0.005$.

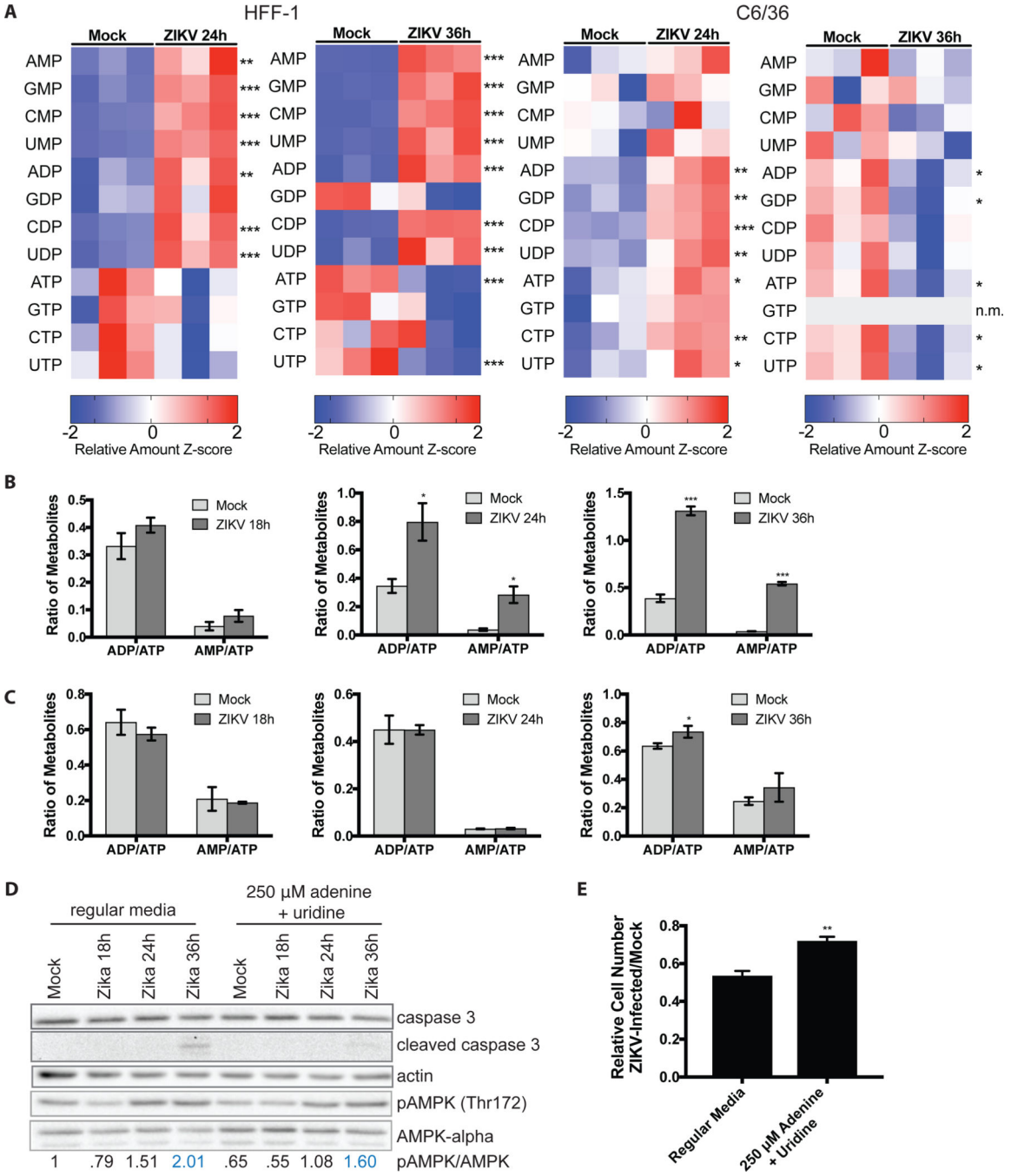


**Figure 3. Zika virus infection selectively depletes nucleotide triphosphates in human but not C6/36 mosquito cells.**

(A) Metabolites were extracted from mock- or ZIKV-infected HFF-1 (left) and C6/36 (right) cells and quantified via LC-MS. Z-scores of the relative amounts of nucleotides are displayed in the heatmaps. (B) AMP/ATP and ADP/ATP ratios in mock- versus ZIKV-infected HFF-1 cells. (C) AMP/ATP and ADP/ATP ratios from mock- versus ZIKV-infected C6/36 cells. (D) Immunoblots from lysates collected from mock- vs. ZIKV-infected HFF-1 cells at indicated time points. Cells were either cultured in normal media (left) or in media supplemented with 250 µM exogenous adenine and uridine (right). Lysates were probed for

total and cleaved caspase 3 levels, pAMPK (Thr172) and AMPK-alpha levels. Actin was used as a loading control. The pAMPK/AMPK ratios are quantified at the bottom as a readout of AMPK activation. (E) HFF-1 cells were mock-infected or ZIKV-infected and cultured in regular vs. adenine and uridine-supplemented media. The relative ZIKV/mock-infected cell counts were measured and displayed in the bar graph. *n.m.* indicates that the metabolite was not measured. Data are represented as mean +/− s.d. *p*-values were calculated using Student's *t*-test and error bars indicate s.d. (n=3), *$p < 0.05$, **$p < 0$ .01, ***$p < 0.005$.

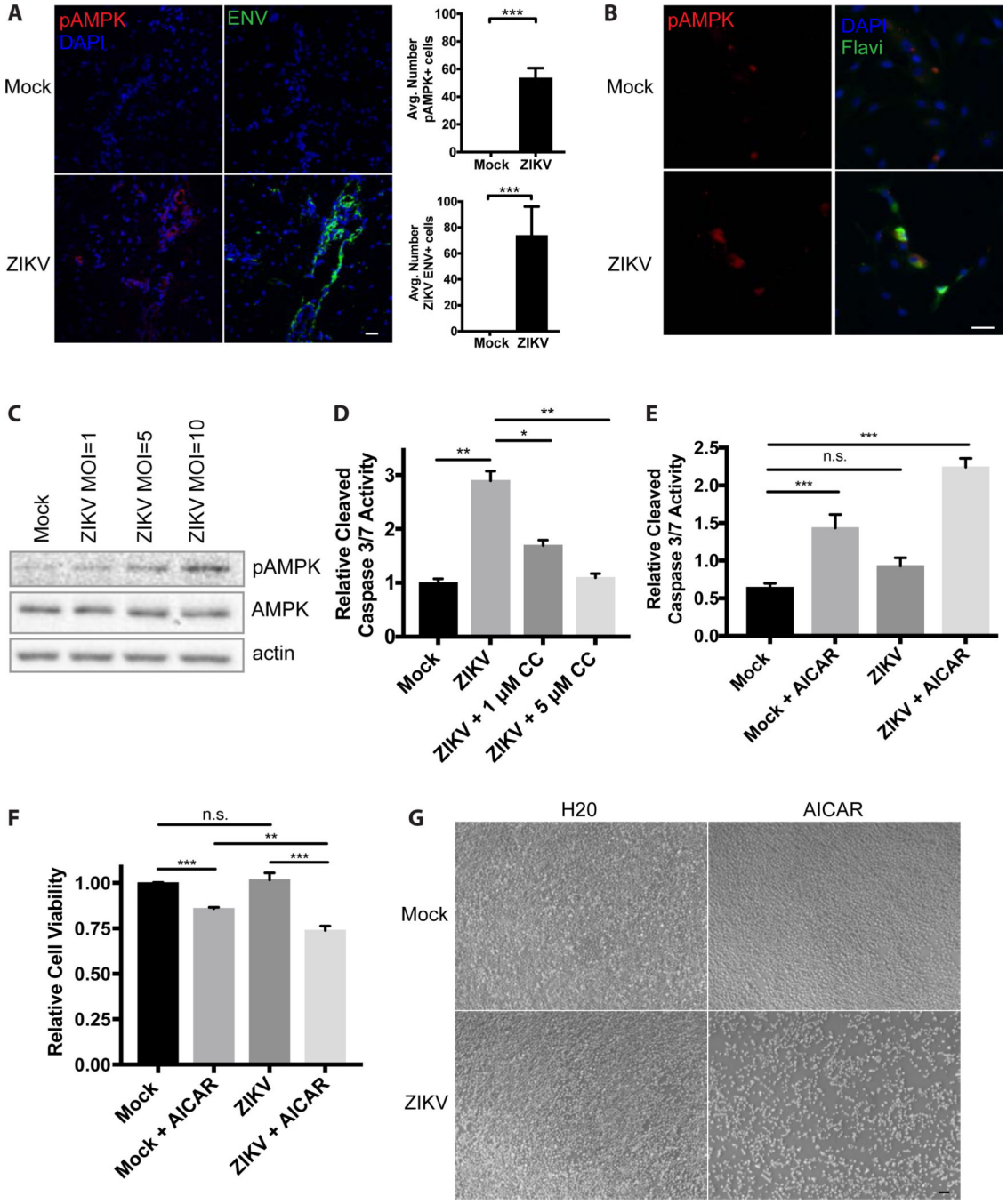


**Figure 4. Zika virus infection increases AMPK phosphorylation and contributes to cell death in clinically relevant models.**

(A) Immunohistochemistry of pAMPK, ZIKV envelope (ENV) protein, and DAPI staining of brain tissue slices from *Ifnar1*−/− mice infected subcutaneously with ZIKV. IHC staining quantification was performed using a series of 4 mouse brain tissue sections per condition and ImageJ software to count cells that stain positive for pAMPK of ZIKV ENV foci. Scale bar, 25 μM. (B) Immunofluoresence of pAMPK, Flavivirus envelope protein (Flavi), and DAPI staining of hFRPE cells 48 hours post-infection with ZIKV at a MOI of 1. Scale bar, 25 μM. (C) pAMPK and AMPK immunoblots on lysates from hFRPE cells mock-infected

and infected by ZIKV at MOIs = 1, 5, 10. Actin was used as a loading control. (D) hFRPE cells were mock- and ZIKV-infected for 48 hours and relative cleaved caspase 3/7 activities were measured in cells that were DMSO-treated or treated with 1 μM and 5 μM Compound C. Data are represented as mean +/− s.d. (E) C6/36 cells were mock-infected or infected with ZIKV at a MOI of 3 and treated with water ($H_20$) or 300 μM AICAR (dissolved in water) for 48 hours and cleaved caspase 3/7 activity was measured 48 hours post-infection or treatment of C6/36 cells. (F) Cell viability measurements were performed using trypan blue exclusion 48 hours post-infection of treatment of C6/36 cells in (E). (G) Light microscope images of C6/36 cells mock-infected or infected with ZIKV taken at 48 hours post-infection. Scale bar, 20 μM.